LETTER

Quantifying 25 years of disease-caused declines in Tasmanian devil populations: host density drives spatial pathogen spread

Calum X. Cunningham,[1]* (iD)
Sebastien Comte,[1,2]
Hamish McCallum,[3]
David G. Hamilton,[1] (iD)
Rodrigo Hamede,[1,4]
Andrew Storfer,[5]
Tracey Hollings,[6,7]
Manuel Ruiz-Aravena,[8]
Douglas H. Kerlin,[3]
Barry W. Brook,[1,10] (iD)
Greg Hocking[9] and
Manna E. Jones[1]

Abstract

Infectious diseases are strong drivers of wildlife population dynamics, however, empirical analyses from the early stages of pathogen emergence are rare. Tasmanian devil facial tumour disease (DFTD), discovered in 1996, provides the opportunity to study an epizootic from its inception. We use a pattern-oriented diffusion simulation to model the spatial spread of DFTD across the species' range and quantify population effects by jointly modelling multiple streams of data spanning 35 years. We estimate the wild devil population peaked at 53 000 in 1996, less than half of previous estimates. DFTD spread rapidly through high-density areas, with spread velocity slowing in areas of low host densities. By 2020, DFTD occupied >90% of the species' range, causing 82% declines in local densities and reducing the total population to 16 900. Encouragingly, our model forecasts the population decline should level-off within the next decade, supporting conservation management focused on facilitating evolution of resistance and tolerance.

Keywords

Approximate Bayesian Computation, density dependence, devil facial tumour disease, disease spread, emerging infectious disease, host-pathogen, integrated species distribution model, *Sarcophilus harrisii*, spatial capture-recapture, wildlife disease.

Ecology Letters (2021) **24**: 958–969

INTRODUCTION

Emerging infectious diseases are a global threat for wildlife (De Castro & Bolker 2005; Skerratt *et al.* 2007; McCallum 2012), leading to cascading ecosystem impacts (McCallum & Dobson 1995; Daszak *et al.* 2000; Buck & Ripple 2017). Understanding the spatial and temporal dynamics of epizootics is key to managing their effects on host populations (Langwig *et al.* 2015; Plowright *et al.* 2019), with variation in host density a major driver of whether epizootics establish in a population and spread to others (Swinton *et al.* 1998; Dobson & Foufopoulos 2001; Hagenaars *et al.* 2004). Simple diffusion models suggest that the velocity of pathogen invasion is determined by factors that influence a pathogen's basic reproductive number (R_0) and/or the movement rate of infected hosts, which can be interrelated (van den Bosch *et al.* 1990, 1992). The processes leading to pathogen transmission can vary with host density and environmental heterogeneity, and can operate at different scales (e.g. within vs. between population spread). For instance, the spatial spread of rabies in racoons was accelerated by unpredictable long-distance dispersal (Russell *et al.* 2005) but slowed by rivers (Smith *et al.* 2002), whereas low host abundance restricted the spread of *Mycoplasma gallisepticum* in house finches (*Carpodacus mexicanus*) (Hosseini *et al.* 2006).

Classic epidemiological models require estimates of pathogen prevalence and transmission, mortality rates and host densities (Anderson & May 1979; McCallum *et al.* 2001), which are difficult to obtain in wild animals (Dobson & Hudson 1995). The difficulty of obtaining this information can be overcome by leveraging ecological data, not necessarily collected for epidemiological purposes, to understand host population dynamics and infer epidemiological processes. Recent advances in species distribution modelling have made it possible to integrate multiple datasets into 'joint-likelihood' models (Miller *et al.* 2019; Isaac *et al.* 2020). These integrative approaches can translate across common ecological data types (Isaac *et al.* 2020), making them highly relevant in an age where large online databases can supplement systematically collected data (Theobald *et al.* 2015; Fletcher Jr. *et al.* 2019).

[1]School of Natural Sciences, University of Tasmania, Private Bag 55, Hobart, TAS 7001, Australia

[2]Vertebrate Pest Research Unit, NSW Department of Primary Industries, 1447 Forest Road, Orange, NSW 2800, Australia

[3]Environmental Futures Research Institute and School of Environment and Science, Griffith University, Nathan, Qld 4111, Australia

[4]CANECEV – Centre de Recherches Ecologiques et Evolutives sur le cancer (CREEC), Montpellier 34090, France

[5]School of Biological Sciences, Washington State University, Pullman, WA 99164-4236, USA

[6]Arthur Rylah Institute for Environmental Research, 123 Brown Street, Heidelberg, Vic. 3084, Australia

[7]School of BioSciences, The University of Melbourne, Parkville, Vic. 3010, Australia

[8]Department of Microbiology and Immunology, Montana State University, Bozeman, MT 59717, USA

[9]Game Services Tasmania, Tasmanian Department of Primary Industries, Parks, Water and Environment, TAS, PO Box 44, Hobart 7001, Australia

[10]ARC Centre of Excellence for Australian Biodiversity and Heritage (CABAH), University of Tasmania, Hobart, Tasmania 7001, Australia

*Correspondence: E-mail: calum.cunningham@utas.edu.au; calumcunningham11@gmail.com

Using multiple datasets can help answer questions where each dataset alone is insufficient (Pacifici *et al.* 2019). Here we use a Bayesian joint-likelihood model (Bachl *et al.* 2019; Isaac *et al.* 2020) to model the long-term population effects of an emerging infectious disease.

The emergence and spread of Tasmanian devil facial tumour disease (DFTD) provides an opportunity to study an epizootic from its inception. DFTD is a transmissible cancer that has caused severe population declines in Tasmanian devils (*Sarcophilus harrisii*, hereafter 'devil') over the last three decades (Hawkins *et al.* 2006; McCallum *et al.* 2007). DFTD was discovered in 1996 and has since spread across most of the devil's geographic range (Hawkins *et al.* 2006; Lazenby *et al.* 2018). The nearly 100% fatal infection causes large tumours on a devil's mouth, face and neck (Fig. 1a), which are transmitted through biting (Pearse & Swift 2006).

Early studies indicated that DFTD transmission is strongly frequency-dependent (McCallum *et al.* 2009), making transmission possible at very low host densities (De Castro & Bolker 2005). This frequency dependence arises because most bite injuries occur during mating interactions when males guard females, which happens irrespective of density (Hamilton *et al.* 2019). The frequency-dependence led early models to suggest the possibility of disease-induced extinction (McCallum *et al.* 2009), and consequently, the species was listed as Endangered (Hawkins *et al.* 2008). While transmission within populations may be maintained by frequency-dependent processes (McCallum *et al.* 2009), we hypothesise here that the initial spatial spread of DFTD might be a density-dependent process at larger spatial scales.

DFTD now encompasses almost the entire geographic range of the devil (i.e. Tasmania, Australia), presenting the opportunity to study the spread and population effects from the first detection of DFTD to maximum potential distribution. Data are available across the entire range of this emerging host-pathogen system from before and during the early stages of the epizootic. We used three datasets: (1) spatiotemporal occurrences of DFTD, (2) 35 years of spotlighting counts of devils, 10 years prior and 25 years after DFTD discovery, and (3) 21 years of longitudinal capture-mark-recapture host density estimates. Our aims and analysis took a two-stage approach (Fig. 1b). Our first aim was to map and model the spatial spread of DFTD across Tasmania, and to investigate how host density influenced the pattern of disease spread. To do this, we developed a stochastic-diffusion simulation that responded to host density. We parameterised this model using a pattern-oriented framework (Grimm *et al.* 2005), providing inference on how host density shaped the spatial spread of DFTD. Our second aim was to model the effects of DFTD on devil density and total abundance. Using a map of DFTD spread as an explanatory variable, we jointly modelled the spotlight counts and capture-mark-recapture data. We forecast these findings to the scenario where DFTD occupies the entire range of the devil (Storfer *et al.* 2017). Finally, we provide the first rigorous estimate of changes in the total abundance of the species.

MATERIALS AND METHODS

Data sources

Spotlight surveys as an index of devil density

The Tasmanian Government has conducted standardised annual spotlighting surveys at up to 172 transects across Tasmania (Fig. 2a; $n = 5761$) from 1985 to 2019 (Table S1). The surveys record all sightings of non-domestic mammalian wildlife species, including devils (Hocking & Driessen 1992), along
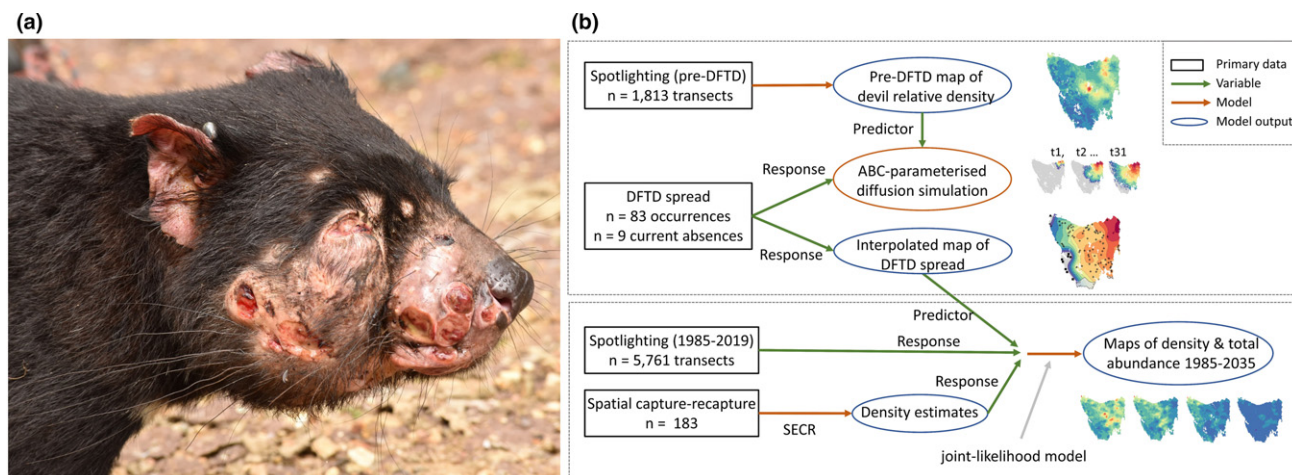

Figure 1 (a) Devil facial tumour disease (DFTD) causes large tumours on the face and mouth of Tasmanian devils (photo: David Hamilton). (b) The main steps involved in our modelling strategy. We first produced maps of the pre-DFTD devil population based on spotlighting data before the discovery of DFTD, and then used this map in a diffusion simulation of DFTD spread across Tasmania (blue box). In a second modelling stage, we used an interpolated map of DFTD spread as a predictor variable in a Bayesian joint-likelihood model, which jointly modelled 35 years of spotlighting data and 21 years of devil density estimates derived from spatially explicit capture-recapture (orange box). From the best joint-likelihood model, we produced maps of devil density, quantified historical changes in the total abundance of the species, and forecasted to the scenario where DFTD will occupy all of the devil's geographic range.

10-km road transects. Transects are driven at a constant speed of 20 km h^{-1}, with one person using a handheld spotlight to observe animals on both sides of the road (for details, see Hocking & Driessen 1992; Hollings *et al.* 2014). Transects are surveyed once per year during the summer months, ensuring comparability between years, but precluding the use of techniques that require repeat surveys within a year, like occupancy modelling. We treat the count of devils per transect as an index of devil density, and henceforth refer to it as 'relative density'.

Estimating absolute density from trapping surveys

We assembled 183 estimates of devil density ($\pm 95\%$ CI) derived from standardised 10-day capture-mark-recapture trapping surveys, which used ~ 40 traps set over 25 km^2 (Appendix S1, Table S2). We first calculated 87 estimates of devil density using spatially explicit capture-recapture (SECR) models (Borchers & Efford 2008). Since SECR uses the spatial detection history to estimate the effective survey area, it can produce comparable estimates of density across different trap layouts (Borchers & Efford 2008). See Appendix S1 for details. In a second step, we combined our results with 96 estimates of devil density reported by Lazenby *et al.* (2018), who also used SECR to estimate density. In total, the density estimates came from 72 298 trap nights at 15 sites (Fig. 2B).

Disease spread

We collated records of DFTD locations including those already published from 1996 to 2015 (Lazenby *et al.* 2018) and recent cases of DFTD in new areas until September 2020. Lazenby *et al.* (2018) reported locations of lab-confirmed DFTD samples until 2015. We additionally used DFTD locations reported in Hawkins *et al.* (2006) and McCallum *et al.* (2007), some of which included cases with clinical signs of DFTD but were not lab-confirmed, which is important before the disease was formally identified. Because we aimed to model the progression of the disease front into new areas, we retained only the earliest arrival of DFTD in each 10×10 km grid cell across Tasmania, leaving 83 records (Fig. 3).

There is little trapping data from south-west Tasmania because the region is largely inaccessible. To survey this area for DFTD, we used records from recent camera-trap surveys. Although cameras are less sensitive for detecting small tumours, they regularly detect tumours when they become larger. In this case, cameras observed tumours in areas with confirmed cases of DFTD but did not detect DFTD along the south-west coast (2016–2020), where live trapping in 2015 also did not detect DFTD. We have therefore included eight absence locations along the south-west coast (Fig. 3). Additionally, one long-term trapping site in the north-west is currently free of disease (Fig. 3). Based on a continuation of the pattern of spread, we estimated that DFTD would arrive at these disease-free sites in 2022 (Fig. 3B). Future disease spread may differ from this estimate, but any departures will have only a small effect on the population estimates because the influence of these data points relates to a small, low-density area of Tasmania.

Modelling spatial data using integrated nested Laplace approximation

We visualised the spatial spread of DFTD and modelled changes in devil density using integrated nested Laplace approximation (INLA) (Illian *et al.* 2013), an accurate and computationally fast option for Bayesian inference from spatial data. We used the inlabru R package (Bachl *et al.* 2019; R Core Team 2019), which builds on the R-INLA package (Rue *et al.* 2009; Bakka *et al.* 2018). Spatial dependence between observations is modelled using a Gaussian random field, which is a spatially continuous process where random variables at any point in space are normally distributed, and are spatially correlated with other random points via a continuous correlation process (Bachl *et al.* 2019). The Gaussian random field is approximated by a stochastic partial differential equation (SPDE) (for details, see Lindgren *et al.* 2011). In all models, we used a Matérn correlation structure for the SPDE (Table S6).

Modelling the pre-DFTD devil population

We spatially modelled devil relative density at the time of DFTD discovery using the count of devils per spotlight transect from 1985 to 1996 as the response variable. We created temporally static continuous variables for the proportional cover of four major habitat classes comprising 84% of Tasmania: (1) wet eucalypt and rainforest (%*wetEuc*, 28% of Tasmania), (2) dry eucalypt forest (%*dryEuc*, 24%), (3) buttongrass moorlands (%*butGrass*, 9%), and (4) agricultural land (%*agric*, 23%). We excluded %*dryEuc* from the models because it was negatively correlated with %*wetEuc* (Pearson's $r = -0.65$). We modelled a non-linear effect of 'survey year' (1985–1996) using a one-dimensional SPDE. Finally, to model spatial correlations not accounted for by covariates, as well as correlations between repeated surveys at a location, we created (1) a temporally static two-dimensional SPDE and (2) a spatiotemporal SPDE. See Table S6 for details and ecological justification of these variables and Fig. S1 for a vegetation map.

We followed the model selection advice of Illian *et al.* (2013) when inferring the effect of spatial covariates in models that also include spatial random fields. We began by fitting a model with the three vegetation covariates and 'survey year'. Using this model, we tested whether devil counts best conformed to a Poisson or negative binomial distribution. Then, we fitted all simpler combinations of the vegetation covariates, aiming to select the statistically important vegetation covariates. Next, we added a temporally static SPDE, and finally a spatiotemporal SPDE (see Table S7 for models). We selected the best model using a leave-one-out cross-validation quantity, the conditional predictive ordinate (CPO), with smaller values of $-2 \times \Sigma(\log CPO)$ indicating better fit (Pettit 1990). To screen for violations of assumptions, we spatially examined CPO scores and histograms of the predictive integral transform, and visually examined Pearson residuals against model estimates (Conn *et al.* 2018). From the best model, we produced a predictive map of devil relative density across Tasmania as a function
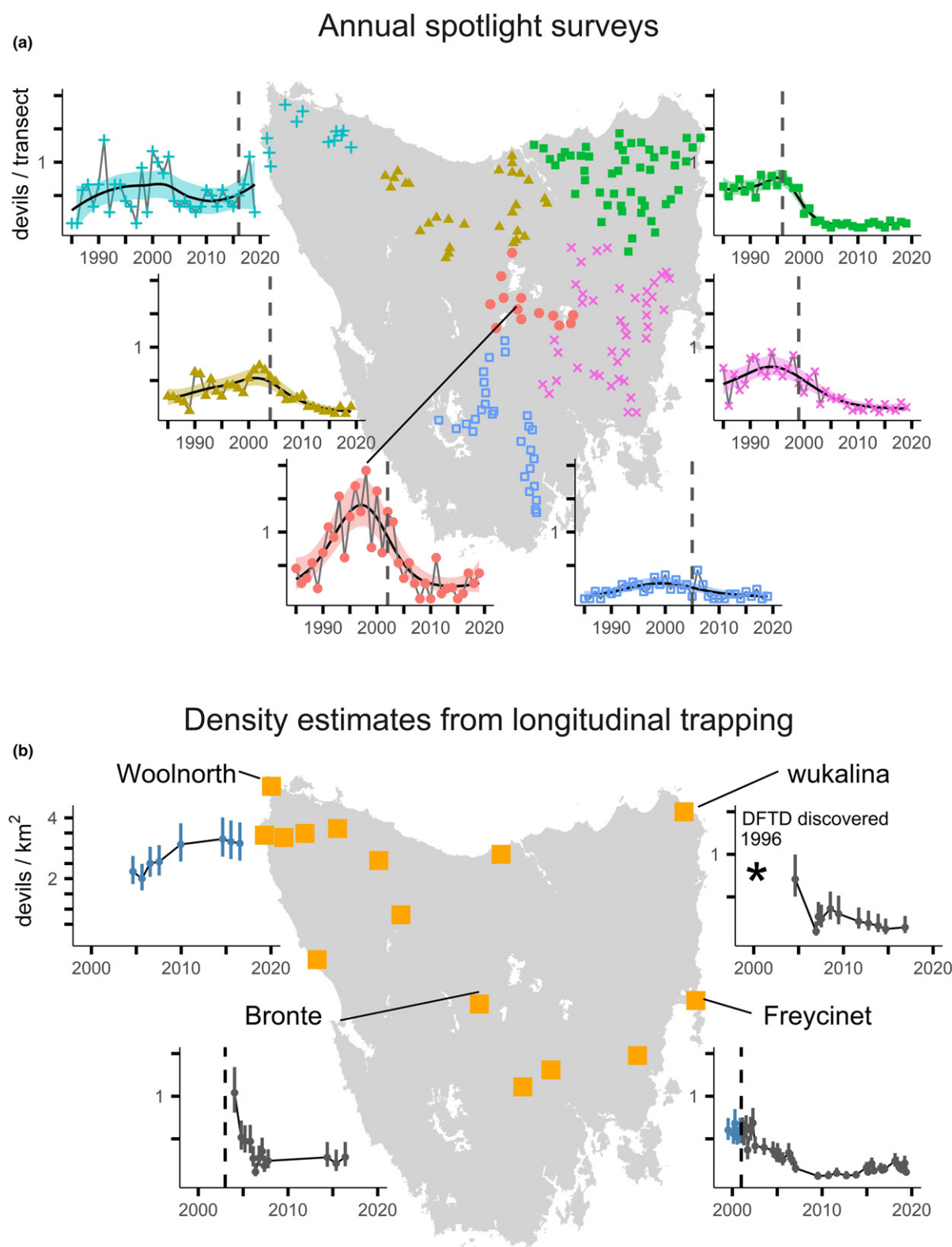
Figure 2 Maps of study sites and trends in the spotlighting and trapping datasets. (a) The map shows the centroids of each of 172 10-km long spotlight transects. To visualise the broad-scale trends in devil detections, we aggregated transects into the national bioregions (IBRA DSEWPC 2013). The data points show the mean number of devil detections within a bioregion. For visualisation purposes only, the trend lines show the mean estimates from a generalised additive model with 95% confidence band. See Fig. S1 for a finer-scale visualisation of the spotlighting data. (b) Yellow squares show the locations of trapping sites, including those reported by Lazenby *et al.* (2018) as well as those analysed in this paper. We present four example time-series of devil densities (95% CI) estimated using spatially explicit capture-recapture, with blue and grey points representing densities before and after the arrival of DFTD respectively. The estimates for Bronte, wukalina and Woolnorth come from Lazenby *et al.* (2018), and we present all density estimates in Fig. S2. In all graphs, the vertical dashed lines denote the approximate year of DFTD arrival to an area. * denotes that disease was discovered at wukalina in 1996, which is earlier than the range of the *x*-axis.

of the vegetation covariates and random field, with year set to 1996. We did this using the predict function of inlabru, which repeatedly draws samples from the posterior distributions of the model parameters.

Pattern-oriented diffusion simulation of the spatial spread of DFTD

To investigate the effect of host density on the spatial spread of DFTD, we developed a grid-based, stochastic-diffusion simulation. We parameterised this model using a pattern-oriented framework, which provides a systematic, data-oriented way of calibrating complex simulation models (Grimm *et al.* 2005; Grimm & Railsback 2012). Specifically, we used Approximate Bayesian Computation (ABC) using the abc package (Csilléry *et al.* 2012) in R. This involved running many versions of the model, each with different parameters drawn from vaguely specified prior distributions. Using summary statistics from the simulations, ABC selects only the models that are close to reproducing 'target' statistics calculated from the observed data, from which ABC estimates the posterior parameter distributions (Csilléry *et al.* 2010; Csilléry *et al.* 2012).

To initiate the simulation, we seeded one grid cell in northeast Tasmania with DFTD at a location between the first two observed cases of DFTD. We started the simulation in 1990 because genomic evidence suggests that although DFTD probably emerged in the 1980s, it was not until the mid-1990s that the effective reproduction number increased and DFTD began to spread more widely (Patton *et al.* 2020). In each of 31 time-steps (1990–2020), the probability of DFTD spreading into an unoccupied grid cell was first determined by the distance, s, from an occupied cell. For cells within s distance, the odds, Y, of DFTD spreading into a cell was:

$$\log(Y) = \beta_1 + \beta_2 relativeDensity,$$

where β_1 is an intercept and β_2 is a coefficient for the effect of devil relative density (previous section). The probability of diffusing into a new cell was stochastically determined by sampling from the binomial distribution with a probability of $\exp(Y)/(1 + \exp(Y))$. We assumed that once grid cells were infected by DFTD, they remained so thereafter, which is broadly true at the landscape scale.

We used ABC to estimate the posterior distributions of s, β_1 and β_2. We considered parameters for β_1 and β_2 to be important if credible intervals did not span zero. We evaluated the simulations on their ability to correctly estimate the year of arrival at 83 DFTD locations and the absence of DFTD in 9 DFTD-free locations. See Appendix S2 for model details and see Appendix S3 for R code.

To visually compare the results of the ABC-parameterised simulation with the observed data, we created an interpolated map of DFTD first cases. Using inlabru (Bachl *et al.* 2019) in R, we modelled the year of DFTD arrival using a Gaussian distribution in response to a spatial random field only (Table S6). From this model, we produced a smooth map of estimated disease-arrival times. Because this model is based solely on a spatial random field, it provides no direct inference about the processes responsible for the pattern of disease spread. Nevertheless, because it directly fits the data, it has higher descriptive fidelity than the diffusion model. We therefore use the diffusion model to interpret the processes driving DFTD spread, while using the random-field-map for the subsequent models investigating population effects.

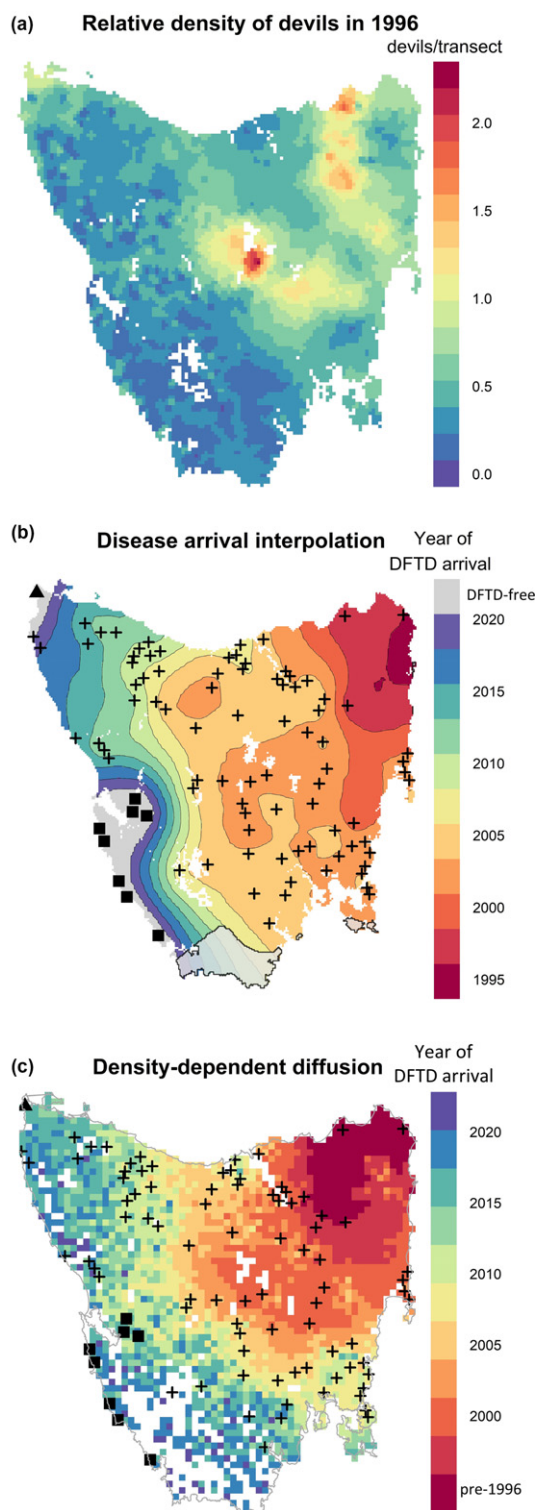## Integrating multiple data sources into a joint-likelihood model

We integrated the density and spotlight datasets into a Bayesian joint-likelihood model. Joint likelihood models combine multiple data sources into single integrated models that estimate a shared set of parameters (Miller *et al.* 2019; Isaac *et al.* 2020). The integrated model has sub-models for each data source, with some or all parameters shared between the sub-models (Bachl *et al.* 2019; Miller *et al.* 2019). We fitted the joint-likelihood model using the inlabru R package (tutorials in Bachl *et al.* 2019; Watson *et al.* 2019). To model spatiotemporal changes to devil density from the spotlighting and density datasets, we created explanatory variables for '*survey year*' (1985–2019) and the model-estimated number of years since DFTD arrival to a site ('*yrsDFTD*'; 0–23 years), which we estimated from the random-field-map of disease spread (Fig. 3B). Non-linear effects of '*survey year*' and '*yrsDFTD*' were modelled using one-dimensional SPDEs (Table S6). As previously described, we modelled the effect of three vegetation types: *%wetEuc*, *%agric* and *%butGrass*. Finally, to model spatial correlations not accounted for by covariates, we included in separate models a temporally static two-dimensional SPDE and a spatiotemporal SPDE that allows the random field to change through time (Table S6).

We followed the same model selection process as for the pre-DFTD model, first by selecting the important environmental covariates, and then adding spatial random fields (Illian *et al.* 2013). For the spotlighting sub-model, the response variable was the count of devils observed on a transect (Poisson or negative binomial distribution). For the density sub-model, the response variable was the estimated devil density for each trapping session (devils/km^2; gamma or Weibull distribution). All models used the default link function. The most complex joint-likelihood model took the form of

$$\log(spotlight) = \beta_1 + f_3(yrsDFTD) + f_4(surveyYear) \\ + \beta_5 wetEuc + \beta_6 butGrass + \beta_7 agric + SPDE$$

$$\log(density) = \beta_2 + f_3(yrsDFTD) \times \beta_8 + f_4(surveyYear) \\ + \beta_5 wetEuc + \beta_6 butGrass + \beta_7 agric + SPDE$$

where β_1 and β_2 are intercepts for each sub-model, f_3 and f_4 are shared non-linear effects, β_5, β_6, β_7 are shared fixed effects, SPDE is a shared spatial random field and β_8 is a scaling constant that modifies f_3 (see chapter 3 of Krainski *et al.* 2019). We included the scaling constant because initial exploration of the two datasets suggested that the spotlight data slightly overstated the decline in devil density. See Table S9 for the structure of all fitted models. From the density sub-model of the best joint model, we produced predictive maps of devil density across Tasmania at various points from 1985 to 2035 (predict function of inlabru). To estimate the total devil abundance, we multiplied density estimates weighted by the area of each grid location across Tasmania. See Appendix S4 for example R code.

(a) Relative density of devils in 1996
devils/transect

(b) Disease arrival interpolation Year of DFTD arrival

(c) Density-dependent diffusion Year of DFTD arrival

Figure 3 After discovery in 1996, the spatial spread of DFTD occurred most rapidly through areas of high devil relative density. The spread of DFTD then appeared to slow as the southern and western disease fronts passed through areas of lower devil relative density. (a) Predictive map of devil spotlighting detections, a proxy for density, at the time of DFTD discovery. This map shows that devils were naturally most abundant in the eastern and central part of Tasmania. The model used data from state-wide spotlight surveys prior to the discovery of DFTD (1985–1996). (b) Map of DFTD spread across Tasmania based on a spatial random field and (c) on a stochastic-diffusion simulation model, incorporating a landscape friction layer based on devil relative density, and parameterised using Approximate Bayesian Computation. The estimated year of disease arrival is shown by colours and contours. Black crosses show the first incidences of lab-confirmed cases of DFTD, or of devils with clinical signs of DFTD. The triangle in the far north-west shows the only remaining long-term trapping site that is currently free of disease, while the squares in the south-west show disease-free areas determined by recent camera trapping. White polygons (b) show inland water bodies. The grey polygon in the south (b) denotes an area with very high uncertainty because of sparse data (standard deviation of at least 3 years; Fig. S4). This area of Tasmania is particularly rugged and has no road access, and consequently very little data from which to infer disease spread.

in the central and eastern part of Tasmania, where vegetation is dominated by dry eucalypt forests and woodlands (Fig. 3A).

The diffusion simulation of DFTD spread suggests that devil density played a key role in mediating the initial spatial spread of DFTD. Within a timestep, the ABC posteriors estimated that DFTD was able to diffuse into grid cells within ~ 18 km of already-occupied cells, with the probability of doing so strongly influenced by the relative devil density of the receiving grid cell ($\beta_{relativeDensity}$ = 7.75, 95% CI: 6.89-8.29) (Table S8; Fig. S5). This model goes some way to explain why DFTD spread south rapidly in the decade after 'break-out', as it moved through an area with high relative densities (Fig. 3). From the mid-2000s, the spread of DFTD was substantially slower, as the western and southern disease-fronts crossed areas of lower relative densities (Fig. 3). The diffusion model correctly predicted that much of south-west Tasmania, a rugged area with low devil densities (Hawkins *et al.* 2006), is currently free of DFTD. The diffusion model and random-field-model estimate that DFTD occupies 91% and 96% of Tasmania (Fig. 3) respectively, with high uncertainty in southern Tasmania, where data is sparse (Fig. S4).

Devil population declines

The joint-likelihood model revealed a strong negative effect of '*yrsDFTD*', with local devil densities declining by an average of 76% 10 years after disease arrival, at which point the population decline tends to level off, with 82% decline after 23 years (Fig. 4C). The joint model revealed a positive effect of '*survey year*', and negative effects of *%but-Grass* and *%wetEuc* (Fig. 4; Table 1; Fig. S6). Devil density was steadily rising before the discovery of DFTD, peaking in 1996 at a Tasmania-wide mean of 0.84 devils/km² (95% CI: 0.61–1.08) and a total population of 53 000 (95% CI: 39 600–71 800) (Fig. 5). By 2020, estimated mean density had declined to 0.27/km² (0.20–0.36) and the total population had declined by 68% to 16 900 (12 500–23 100) (Fig. 5).
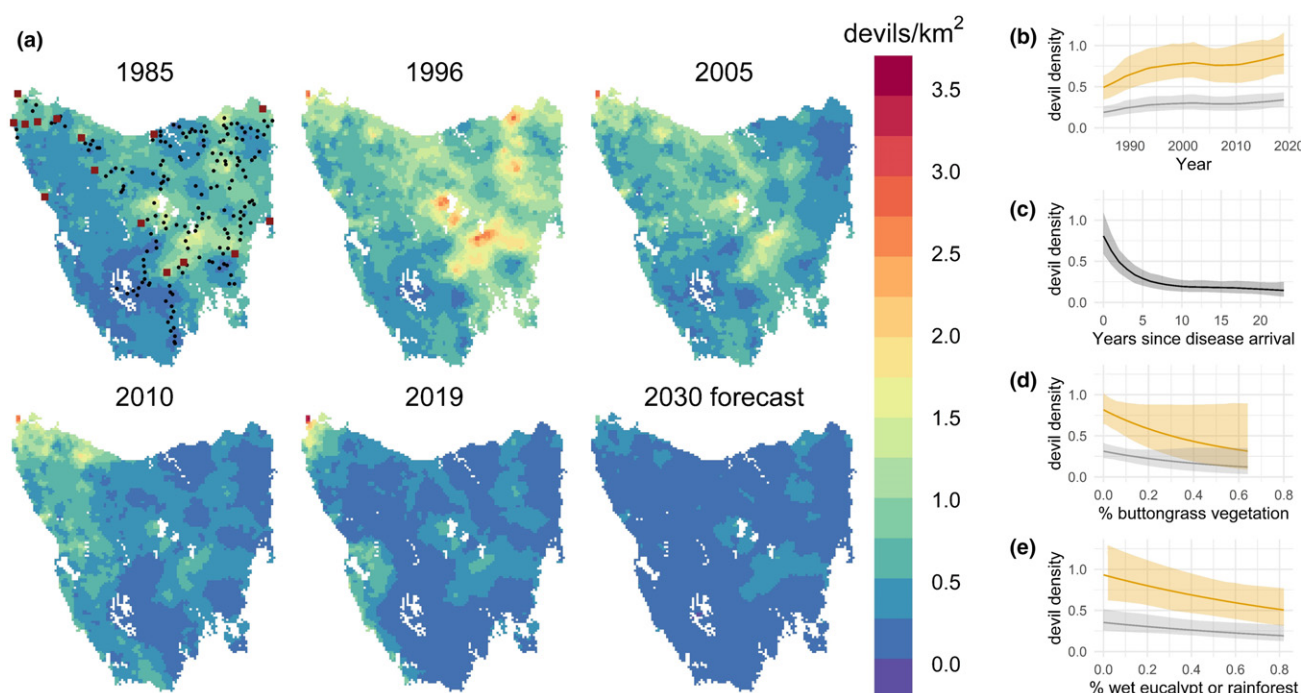
RESULTS

Density-dependent spatial spread of DFTD

Devil relative density varied substantially across Tasmania at the time of DFTD discovery (Fig. 3A). The best model of pre-DFTD spotlight detections included a spatiotemporal random field and negative effects of wet eucalypt/rainforest and button-grass (Table S7). As a result, devil relative density was highest

Figure 4 (a) Predictive maps of Tasmanian devil density from the joint-likelihood model. Devil densities were rising before the discovery of DFTD in 1996. The spread of DFTD across Tasmania then caused a wave of rapid and severe population declines. In the first panel (only), black dots indicate the location of annual spotlight transects and maroon squares show the location of longitudinal trapping sites. See Fig. S7 for maps of uncertainty around the density estimates. (b–e) The effect of predictor variables on devil density from the best joint-likelihood model (±95% credible interval). Grey lines show the effect of a predictor variable across its range when all other predictors are held at their mean (i.e. 4.5 years after the arrival of DFTD), and yellow lines show the effect when sites were free of DFTD. The axis ranges reflect the range of those variables.

Table 1 Model selection table for the joint-likelihood model, which simultaneously modelled devil density at long-term trapping sites and devil detections on long-term spotlight transects. Here we present the four top-performing models and a null model. We selected the best model based on a leave-one-out cross-validation metric, the conditional predictive ordinate (CPO), with ΔCPO showing the difference from the best model. We present the mean coefficient estimate, with 95% credible interval shown in brackets. 'nl' denotes a non-linear effect. All models in this table used the gamma distribution to model density and the negative binomial distribution to model the spotlight counts. See Table S9 for the full model selection table.

Model	$-2 \times$ $\Sigma(\log CPO)$	ΔCPO	Intercept: spotlight sub-model	Intercept: density sub-model	Year	Years since DFTD arrival	Scaling constant	% button grass	% wet eucalypt/ rainforest	% agric	Gaussian random field
1	**7570.5**	**0.0**	**2.61** **(−3.46, −1.92)**	**−1.58** **(−2.3, −0.96)**	**nl**	**nl**	**0.70** **(0.59, 0.81)**	**−1.88** **(−3.65, −0.19)**	**−0.80** **(−1.37, −0.24)**		**✓**
2	7571.2	0.7	−2.59 (−3.48, −1.86)	−1.57 (−2.31, −0.91)	nl	nl	0.70 (0.59, 0.81)	−1.91 (−3.71, −0.18)	−0.82 (−1.43, −0.20)	−0.05 (−0.67, 0.57)	✓
3	8036.3	465.8	−2.64 (−3.80, −1.94)	−1.53 (−2.42, −0.94)	nl	nl	0.76 (0.62, 0.89)	−1.05 (−1.74, −0.37)	−0.86 (−1.07, −0.65)	0.27 (0.01, 0.54)	
4	8038.7	468.1	−2.57 (−3.75, −1.86)	−1.48 (−2.41, −0.88)	nl	nl	0.78 (0.64, 0.92)	−1.28 (−1.94, −0.61)	−0.93 (−1.14, −0.73)		
Null	8884.5	1314.0	−1.07 (−1.12, −1.01)	−0.49 (−0.60, −0.37)							

To project forward to the scenario where DFTD will occupy all of Tasmania, we made the simplifying assumption, based on a continuation of disease spread trends, that DFTD will occupy all of Tasmania by 2022. Based on this assumption, our model forecasts a continuing but slowing decline of total devil abundance (Fig. 5), suggesting it should plateau at 11 900 devils (95% CI: 6300–18 600). Overall, this would represent a 78% decline in total abundance. To date, no local

extinctions have been documented, with devil populations persisting at all monitoring sites, albeit at much lower densities (Fig. S2).

DISCUSSION

We modelled the spread of an infectious epizootic disease, DFTD, from emergence until the present, where it now
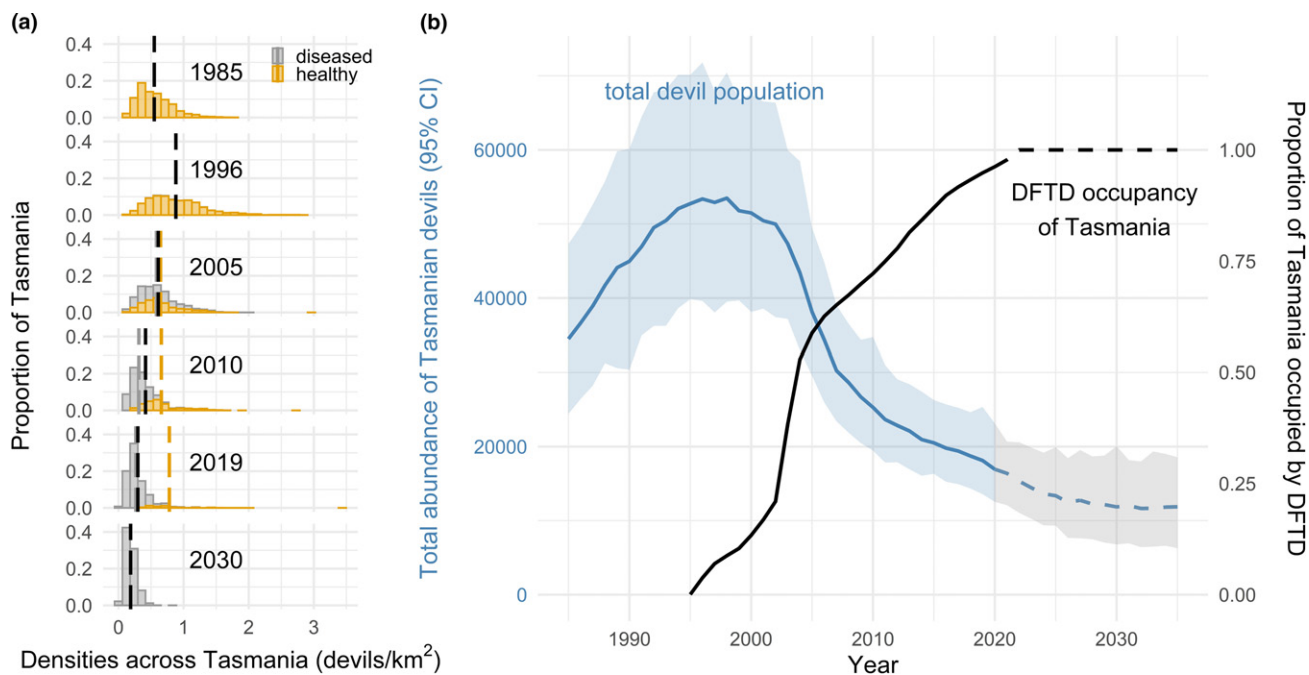
Figure 5 Changes in the Tasmanian devil population across the entire geographic range of the species. (a) Estimates of devil density across Tasmania at time points from 1985 and 2030. Yellow bars distinguish density in areas that are free of DFTD and grey shows densities where DFTD is present. The vertical dashed lines show the mean density in each disease category, with black denoting the overall mean. (b) Changes in the global abundance (±95% credible interval) of Tasmanian devils. Dashed lines represent forecasts into the future. The black line shows the estimated proportion of Tasmania occupied by DFTD based on the random-field-model of disease spread (Fig. 3b).

occupies > 90% of the geographic range of its sole host, the Tasmanian devil. DFTD emerged in an area of high host density, potentially creating the perfect conditions for the epizootic to establish and spread, with our diffusion simulation suggesting that DFTD spread fastest in areas of high host density. We integrated 35 years of spotlighting data and 21 years of capture-mark-recapture data to spatially model changes in the devil population, highlighting the utility of recent advances in data integration for modelling changes to species' distributions (Miller *et al.* 2019; Isaac *et al.* 2020). The joint-likelihood model allowed us to quantify, for the first time, the wave of severe population declines as DFTD invaded host populations. Our forecast, which does not include rapid evolutionary dynamics, predicts the devil population decline is likely to level-off within the next decade.

Density-dependent spatial spread of DFTD

Our pattern-oriented diffusion simulation suggests that DFTD spread most rapidly through areas of high host density. This raises an interesting point about spatial scale: although transmission within devil populations may be maintained by frequency-dependent processes (McCallum *et al.* 2009), the spatial spread of DFTD was apparently density-dependent. Using a simple diffusion model, van den Bosch *et al.* (1992) show that the spread of an invading organism is driven by a combination of the host movement rate and the intrinsic rate of increase. Both movement rate and interactions between devils could increase in response to competition. At high devil

densities, carrion and live prey are less available *per capita* (Cunningham *et al.* 2018) and aggressive interactions at carcasses are more common (Hamede *et al.* 2008). Female devils in high density populations have larger home ranges (Comte *et al.* 2020) and disperse larger distances (Lachish *et al.* 2011; Storfer *et al.* 2017). Other studies, for instance of European badgers, show that larger home ranges can lead to increased potential for pathogen transmission (Woodroffe *et al.* 2006), and simulations show that greater host movement can increase the probability of a pandemic establishing (Cross *et al.* 2005). Adult devils sometimes engage in long-distance excursions of ~ 15–25 km (M. Jones, unpublished tracking data). These are likely to be more numerous at high densities, and could act as rare long-distance transmission events, which have been shown in other systems to substantially accelerate disease spread (Smith *et al.* 2002; Russell *et al.* 2005; Smith *et al.* 2005; Meentemeyer *et al.* 2011). Our simulation model was a first step in establishing a probable link between host density and the spatial spread of DFTD. Future studies should unpick the mechanisms that depend on density, and incorporate other drivers or barriers of DFTD spread, both of which would likely require a finer scale of study that matches the scale of transmission and host movement.

Population trends and conservation

Our estimate of pre-DFTD devil population size is less than half the previous estimate of 130 000–150 000 (Hawkins *et al.* 2008), which would require average densities across Tasmania of 2.15 devils/km². Our estimates suggest that only 1.3% of

Tasmania had densities of at least 2.15 devils/km^2 at the time of DFTD discovery (Fig. 5B). This discrepancy might have two main causes. First, SECR has produced smaller density estimates than older methods. SECR uses the spatial detection histories of animals to estimate the effective sampling area (Borchers & Efford 2008), which can differ substantially between similar-sized trapping arrays (Table S5). In contrast, older methods defined the sampling area based on a buffer around trap sites without considering how animal movement around study sites influences the effective survey area (Hawkins *et al.* 2008). Second, previous extrapolations seemingly suffered from a common form of site selection bias, whereby study sites are selected in high-density areas (Fournier *et al.* 2019). Extrapolating such density estimates to areas with lower suitability, such as the Tasmanian south-west (Jones & Rose 1996; Hawkins *et al.* 2006), is likely to result in an over-estimated population size. The integration of multiple datasets in our analysis allowed us to incorporate information from a broader range of environments, including low-suitability habitat, while harnessing the favourable qualities of each dataset (high-quality density estimates and long-term, wide-spread spotlight counts).

Based on the persistence of devils at all long-term diseased sites, our model predicts the overall population is likely to stabilise within the next 10 years. This supports recent simulations suggesting the most likely long-term outcomes are either the coexistence of devils and DFTD, or DFTD fading out (Wells *et al.* 2019), with genomic evidence suggesting a transition towards endemism (Patton *et al.* 2020). These stabilising trends reflect a growing body of research suggesting that devils are potentially adapting to DFTD in the face of this extreme selective pressure (Epstein *et al.* 2016; Ruiz-Aravena *et al.* 2018; Margres *et al.* 2018a; Fraik *et al.* 2020). Several individual devils have demonstrated natural tumour regressions in association with an immune response (Pye *et al.* 2016a), with tumour regression potentially related to genomic variation in both host (Margres *et al.* 2018b) and tumour (Margres *et al.* 2020). Nevertheless, it remains unclear how the genomic changes detected in long-term diseased areas (Epstein *et al.* 2016) relate to functional traits in devil-DFTD interactions, and whether genomic changes are involved in the persistence and even recovery of some populations.

Despite revealing 25 years of ongoing population decline, our results suggest the species no longer meets the criteria for Endangered status under the IUCN Red List. Because the Red List evaluates population reductions over the longer of 10 years or three generations (IUCN Standards & Petitions Committee 2019), the severe devil population decline before 2010 is essentially excluded from consideration. Our modelling suggests the species now qualifies for Vulnerable status based on a 31% population decline from 2011 to 2020 (criterion A2), and a reproductively mature population size that is likely to be < 10 000 but > 2500 individuals within the next decade (criterion C1). Given the population has declined by 68% over the last 25 years, numbers continue to decline, and the trend is not reversible with current knowledge, we strongly caution that the potential down-listing of the species does not mean the species is secure. This is particularly so in the face of new and uncertain threats, including the discovery in 2014

of a second, independently evolved facial tumour (DFT2) which is spreading through southern Tasmania (Pye *et al.* 2016b; James *et al.* 2019).

Although the outlook for the wild devil population is undoubtedly more positive than it was a decade ago (McCallum *et al.* 2009), devils are currently well below ecologically functional densities across much of Tasmania. Devil declines have had cascading ecological effects, such as carrion accumulation (Cunningham *et al.* 2018), mesopredator release with effects on small and medium-sized mammals (Hollings *et al.* 2014; Hollings *et al.* 2016; Cunningham *et al.* 2020), and the relaxation of anti-predator behaviours by prey (Hollings *et al.* 2015; Cunningham *et al.* 2019a; Cunningham *et al.* 2019b). In the the online data repository, we provide annual rasters of estimated devil densities from 1985 to 2035, which we expect will be useful for improving our understanding of the ecological effects of devils and identifying thresholds that could provide longer term targets for population recovery.

Given DFTD-induced extinction of the devil now seems unlikely, we suggest several management priorities. First, we emphasise the importance of continued monitoring across the species' geographic range, particularly following the discovery of DFT2 (Pye *et al.* 2016b). Second, because the now-small devil population is more exposed to other threatening processes (De Castro & Bolker 2005; McCallum 2012), it is an ongoing priority to minimise additional stressors like vehicle collisions and habitat destruction. A third exciting priority is that we can attempt to accelerate the pace of evolution by identifying and then moving advantageous genotypes to areas lacking them (McCallum 2012). Crucially, these genotypes need to come from populations that are under selective pressure by DFTD (Hohenlohe *et al.* 2019; Hamede *et al.* 2020). It is, however, important to recognise the potential for DFTD to evolve in response to changes in the host population, and that selecting for resistant devils might inadvertently select for more virulent tumours. Before intervening to boost adaptation, it is therefore important to better understand (1) how genotype influences phenotype in both devils and DFTD, and (2) how these traits influence the persistence of devils in long-diseased populations.

Concluding remarks

Modelling spatial dynamics of pathogens in wildlife populations remains a major challenge (White *et al.* 2018), but is critical for managing emerging disease threats, both to wildlife themselves and to human or livestock populations to which these pathogens may spill over. Our study of DFTD as it has spread across almost the entire geographic range of its sole host takes advantage of recent advances in pattern-oriented modelling, as well as joint modelling of multiple datasets. Diffusion-based approaches are often considered to be high-level general frameworks not well suited to providing specific predictions (White *et al.* 2018). By re-imagining a diffusion model as a multi-layer, grid-based simulation, our framework can accommodate complex processes that would otherwise be intractable using an analytical diffusion model. Our highly flexible simulation shows that diffusion-based models can provide explicit quantitative information on the relationship

between host density and spatial spread, which should have broad, real-world applications to other wildlife disease systems, and invading organisms more generally. Ours is, however, one of few studies of emerging infectious diseases with plentiful 'spatiotemporal data on both host and pathogen populations from the time of disease emergence. This highlights the importance of long-term monitoring programs. Regular, joint analysis of general-purpose survey datasets that monitor a large suite of species would be valuable for the early detection of population declines or disease emergence at a point where management interventions can be effective. Our analysis involved the use of survey data that was established to monitor harvested herbivore species, but has now provided valuable insights into the influence of host density on infectious disease spread and the population effects of an emerging infectious disease that did not exist when the surveys were established.

ETHICS STATEMENT

This study was conducted in accordance with the Univ. of Tasmania Animal Ethics Committee permits A0008588, A0010296, A0011696, A0013326, A0015835, A0018223 and A0016789.

AUTHORSHIP

CXC, MEJ, SC and HM conceived of the idea for the paper. CXC did the spatial modelling, SC and CXC conducted the SECR analysis, and CXC and BB developed the simulation model. SC, DH, MR and RH contributed trapping data, and GH contributed the spotlighting data. CXC wrote the first draft, and all authors contributed to writing thereafter. MEJ, HM, AS and RH obtained funding for the trapping fieldwork.

PEER REVIEW

The peer review history for this article is available at https://publons.com/publon/10.1111/ele.13703.

DATA AVAILABILITY STATEMENT

The data supporting the results have been archived in the Dryad public data repository (https://doi.org/10.6084/m9.figshare.13624406.v1; https://doi.org/10.6084/m9.figshare.13624517.v1; https://doi.org/10.6084/m9.figshare.13624565.v1; https://doi.org/10.6084/m9.figshare.13728220).

REFERENCES

Anderson, R.M. & May, R.M. (1979). Population biology of infectious diseases: Part I. *Nature*, 280, 361–367.

Bachl, F.E., Lindgren, F., Borchers, D.L. & Illian, J.B. (2019). inlabru: an R package for Bayesian spatial modelling from ecological survey data. *Methods Ecol. Evol.*, 10, 760–766.

Bakka, H., Rue, H., Fuglstad, G.-A., Riebler, A., Bolin, D., Illian, J. et al. (2018). Spatial modeling with R-INLA: a review. *WIREs Computational Statistics*, 10, e1443.

Borchers, D.L. & Efford, M.G. (2008). Spatially explicit maximum likelihood methods for capture-recapture studies. *Biometrics*, 64, 377–385.

van den Bosch, F., Hengeveld, R. & Metz, J.A.J. (1992). Analysing the velocity of animal range expansion. *J. Biogeogr.*, 19, 135–150.

van den Bosch, F., Metz, J.A.J. & Diekmann, O. (1990). The velocity of spatial population expansion. *J. Math. Biol.*, 28, 529–565.

Buck, J.C. & Ripple, W.J. (2017). Infectious agents trigger trophic cascades. *Trends Ecol. Evol.*, 32, 681–694.

Comte, S., Carver, S., Hamede, R. & Jones, M. (2020). Changes in spatial organization following an acute epizootic: Tasmanian devils and their transmissible cancer. *Glob. Ecol. Conserv.*, 22, e00993.

Conn, P.B., Johnson, D.S., Williams, P.J., Melin, S.R. & Hooten, M.B. (2018). A guide to Bayesian model checking for ecologists. *Ecol. Monogr.*, 88, 526–542.

Cross, P.C., Lloyd-Smith, J.O., Johnson, P.L.F. & Getz, W.M. (2005). Duelling timescales of host movement and disease recovery determine invasion of disease in structured populations. *Ecol. Lett.*, 8, 587–595.

Csilléry, K., Blum, M.G.B., Gaggiotti, O.E. & François, O. (2010). Approximate Bayesian Computation (ABC) in practice. *Trends Ecol. Evol.*, 25, 410–418.

Csilléry, K., François, O. & Blum, M.G.B. (2012). abc: an R package for approximate Bayesian computation (ABC). *Methods Ecol. Evol.*, 3, 475–479.

Cunningham, C.X., Johnson, C.N., Barmuta, L.A., Hollings, T., Woehler, E. & Jones, M.E. (2018). Top carnivore decline has cascading effects on scavengers and carrion persistence. *Proc. R. Soc. B*, 285, 20181582.

Cunningham, C.X., Johnson, C.N., Hollings, T., Kreger, K. & Jones, M.E. (2019a). Trophic rewilding establishes a landscape of fear: Tasmanian devil introduction increases risk-sensitive foraging in a key prey species. *Ecography*, 42(12), 2053–2059.

Cunningham, C.X., Johnson, C.N. & Jones, M.E. (2020). A native apex predator limits an invasive mesopredator and protects native prey:

Tasmanian devils protecting bandicoots from cats. *Ecol. Lett.*, 23(4), 711–721.

Cunningham, C.X., Scoleri, V., Johnson, C.N., Barmuta, L.A. & Jones, M. (2019b). Temporal partitioning of activity: rising and falling top-predator abundance triggers community-wide shifts in diel activity. *Ecography*, 42(12), 2157–2168.

Daszak, P., Cunningham, A.A. & Hyatt, A.D. (2000). Emerging infectious diseases of wildlife– threats to biodiversity and human health. *Science*, 287, 443–449.

De Castro, F. & Bolker, B. (2005). Mechanisms of disease-induced extinction. *Ecol. Lett.*, 8, 117–126.

Dobson, A. & Foufopoulos, J. (2001). Emerging infectious pathogens of wildlife. *Philos. Trans. R. Soc. Lond. B Biol. Sci.*, 356, 1001–1012.

Dobson, A. & Hudson, P. (1995). Microparasites: observed patterns in wild animal populations. In: *Ecology of infectious diseases in natural populations* (eds. Grenfell, B. & Dobson, A.). Cambridge University Press, Cambridge, p. 89.

Epstein, B., Jones, M., Hamede, R., Hendricks, S., McCallum, H., Murchison, E.P. *et al.* (2016). Rapid evolutionary response to a transmissible cancer in Tasmanian devils. *Nat. Commun.*, 7, 12684.

Fletcher Jr, R.J., Hefley, T.J., Robertson, E.P., Zuckerberg, B., McCleery, R.A. & Dorazio, R.M. (2019). A practical guide for combining data to model species distributions. *Ecology*, 100, e02710.

Fournier, A.M.V., White, E.R. & Heard, S.B. (2019). Site-selection bias and apparent population declines in long-term studies. *Conserv. Biol.*, 33, 1370–1379.

Fraik, A.K., Margres, M.J., Epstein, B., Barbosa, S., Jones, M., Hendricks, S. *et al.* (2020). Disease swamps molecular signatures of genetic-environmental associations to abiotic factors in Tasmanian devil (*Sarcophilus harrisii*) populations. *Evolution*, 74(7), 1392–1408.

Grimm, V. & Railsback, S.F. (2012). Pattern-oriented modelling: a multi-scope for predictive systems ecology. *Philos. Trans. R. Soc. Lond. B Biol. Sci.*, 367, 298–310.

Grimm, V., Revilla, E., Berger, U., Jeltsch, F., Mooij, W.M., Railsback, S.F. *et al.* (2005). Pattern-oriented modeling of agent-based complex systems: lessons from ecology. *Science*, 310, 987.

Hagenaars, T.J., Donnelly, C.A. & Ferguson, N.M. (2004). Spatial heterogeneity and the persistence of infectious diseases. *J. Theor. Biol.*, 229, 349–359.

Hamede R., Madsen T., McCallum H., Storfer A., Hohenlohe P.A., Siddle H. *et al.* (2020) Darwin, the devil, and the management of transmissible cancers. *Conservation Biology*, http://dx.doi.org/10.1111/cobi.13644.

Hamede, R.K., McCallum, H. & Jones, M. (2008). Seasonal, demographic and density-related patterns of contact between Tasmanian devils (*Sarcophilus harrisii*): Implications for transmission of devil facial tumour disease. *Austral Ecol.*, 33, 614.

Hamilton, D.G., Jones, M.E., Cameron, E.Z., McCallum, H., Storfer, A., Hohenlohe, P.A. *et al.* (2019). Rate of intersexual interactions affects injury likelihood in Tasmanian devil contact networks. *Behav. Ecol.*, 30 (4), 1087–1095.

Hawkins, C.E., Baars, C., Hesterman, H., Hocking, G.J., Jones, M.E., Lazenby, B. *et al.* (2006). Emerging disease and population decline of an island endemic, the Tasmanian devil *Sarcophilus harrisii*. *Biol. Cons.*, 131, 307–324.

Hawkins, C.E., McCallum, H., Mooney, N., Jones, M. & Holdsworth, M. (2008). *Sarcophilus harrisii*. The IUCN Red List of Threatened Species 2008: e.T40540A10331066. https://doi.org/10.2305/IUCN.UK. 2008.RLTS.T40540A10331066.en.

Hocking, G.J. & Driessen, M.M. (1992). *Tasmanian Spotlight Survey Manual: A Set of Instructions and Maps for Conducting Spotlight Surveys in Tasmania*. Department of Parks Wildlife and Heritage, Hobart.

Hohenlohe, P.A., McCallum, H.I., Jones, M.E., Lawrance, M.F., Hamede, R.K. & Storfer, A. (2019). Conserving adaptive potential: lessons from Tasmanian devils and their transmissible cancer. *Conserv. Genet.*, 20, 81–87.

Hollings, T., Jones, M., Mooney, N. & McCallum, H. (2014). Trophic cascades following the disease-induced decline of an apex predator, the Tasmanian devil. *Conserv. Biol.*, 28, 63–75.

Hollings, T., Jones, M., Mooney, N. & McCallum, H.I. (2016). Disease-induced decline of an apex predator drives invasive dominated states and threatens biodiversity. *Ecology*, 97, 394–405.

Hollings, T., McCallum, H., Kreger, K., Mooney, N. & Jones, M. (2015). Relaxation of risk-sensitive behaviour of prey following disease-induced decline of an apex predator, the Tasmanian devil. *Proc. R. Soc. B*, 282, 20150124.

Hosseini, P.R., Dhondt, A.A. & Dobson, A.P. (2006). Spatial spread of an emerging infectious disease: conjunctivitis in house finches. *Ecology*, 87, 3037–3046.

IBRA DSEWPC (2013). Interim Biogeographic Regionalisation for Australia (IBRA), Version 7 (Regions).

Illian, J.B., Martino, S., Sørbye, S.H., Gallego-Fernández, J.B., Zunzunegui, M., Esquivias, M.P. *et al.* (2013). Fitting complex ecological point process models with integrated nested Laplace approximation. *Methods Ecol. Evol.*, 4, 305–315.

Isaac, N.J.B., Jarzyna, M.A., Keil, P., Dambly, L.I., Boersch-Supan, P.H., Browning, E. *et al.* (2020). Data integration for large-scale models of species distributions. *Trends Ecol. Evol.*, 35, 56–67.

IUCN Standards and Petitions Committee (2019). *Guidelines for Using the IUCN Red List Categories and Criteria*. http://www.iucnredlist.org/documents/RedListGuidelines.pdf.

James, S., Jennings, G., Kwon, Y.M., Stammnitz, M., Fraik, A., Storfer, A. *et al.* (2019). Tracing the rise of malignant cell lines: Distribution, epidemiology and evolutionary interactions of two transmissible cancers in Tasmanian devils. *Evol. Appl.*, 12, 1772–1780.

Jones, M.E. & Rose, R.K. (1996). *Preliminary Assessment of Distribution and Habitat Associations of the Spotted-Tailed Quoll (*Dasyurus maculatus maculatus*) and Eastern Quoll (*D. viverrinus*) in Tasmania to Determine Conservation and Reservation Status*. Tasmanian Public Land Use Commission, Hobart, Tasmania.

Krainski, E.T., Gómez-Rubio, V., Bakka, H., Lenzi, A., Castro-Camilo, D., Simpson, D. *et al.* (2019). Chapter 3: More than one likelihood. In: *Advanced Spatial Modeling with Stochastic Partial Differential Equations Using R and INLA*. CRC Press/Taylor and Francis Group. https://becarioprecario.bitbucket.io/spde-gitbook/ch-manipula.html.

Lachish, S., Miller, K.J., Storfer, A., Goldizen, A.W. & Jones, M.E. (2011). Evidence that disease-induced population decline changes genetic structure and alters dispersal patterns in the Tasmanian devil. *Heredity*, 106, 172–182.

Langwig, K.E., Voyles, J., Wilber, M.Q., Frick, W.F., Murray, K.A., Bolker, B.M. *et al.* (2015). Context-dependent conservation responses to emerging wildlife diseases. *Front. Ecol. Environ.*, 13, 195–202.

Lazenby, B.T., Tobler, M.W., Brown, W.E., Hawkins, C.E., Hocking, G.J., Hume, F. *et al.* (2018). Density trends and demographic signals uncover the long-term impact of transmissible cancer in Tasmanian devils. *J. Appl. Ecol.*, 55, 1368–1379.

Lindgren, F., Rue, H. & Lindström, J. (2011). An explicit link between Gaussian fields and Gaussian Markov random fields: the stochastic partial differential equation approach. *J. R. Stat. Soc. Series B Stat. Methodol.*, 73, 423–498.

Margres, M.J., Jones, M.E., Epstein, B., Kerlin, D.H., Comte, S., Fox, S. *et al.* (2018a). Large-effect loci affect survival in Tasmanian devils (*Sarcophilus harrisii*) infected with a transmissible cancer. *Mol. Ecol.*, 27, 4189–4199.

Margres, M.J., Ruiz-Aravena, M., Hamede, R., Jones, M.E., Lawrance, M.F., Hendricks, S.A. *et al.* (2018b). The genomic basis of tumor regression in Tasmanian Devils (*Sarcophilus harrisii*). *Genome Biology and Evolution*, 10, 3012–3025.

Margres, M.J., Ruiz-Aravena, M., Hamede, R., Chawla, K., Patton, A.H., Lawrance, M.F. *et al.* (2020). Spontaneous tumor regression in Tasmanian devils associated with RASL11A activation. *Genetics*, 215 (4), 1143–1152.

McCallum, H. (2012). Disease and the dynamics of extinction. *Philos. Trans. R. Soc. B Biol. Sci.*, 367, 2828–2839.

McCallum, H., Barlow, N. & Hone, J. (2001). How should pathogen transmission be modelled? *Trends Ecol. Evol.*, 16, 295–300.

McCallum, H. & Dobson, A. (1995). Detecting disease and parasite threats to endangered species and ecosystems. *Trends Ecol. Evol.*, 10, 190–194.

McCallum, H., Jones, M., Hawkins, C., Hamede, R., Lachish, S., Sinn, D.L. *et al.* (2009). Transmission dynamics of Tasmanian devil facial tumor disease may lead to disease-induced extinction. *Ecol.*, 90, 3379–3392.

McCallum, H., Tompkins, D.M., Jones, M., Lachish, S., Marvanek, S., Lazenby, B. *et al.* (2007). Distribution and impacts of tasmanian devil facial tumor disease. *EcoHealth*, 4, 318–325.

Meentemeyer, R.K., Cunniffe, N.J., Cook, A.R., Filipe, J.A.N., Hunter, R.D., Rizzo, D.M. *et al.* (2011). Epidemiological modeling of invasion in heterogeneous landscapes: spread of sudden oak death in California (1990–2030). *Ecosphere*, 2(2), 1990–2030.

Miller, D.A.W., Pacifici, K., Sanderlin, J.S. & Reich, B.J. (2019). The recent past and promising future for data integration methods to estimate species' distributions. *Methods Ecol. Evol.*, 10, 22–37.

Pacifici, K., Reich, B.J., Miller, D.A.W. & Pease, B.S. (2019). Resolving misaligned spatial data with integrated species distribution models. *Ecology*, 100, e02709.

Patton, A.H., Lawrance, M.F., Margres, M.J., Kozakiewicz, C.P., Hamede, R., Ruiz-Aravena, M. *et al.* (2020). A transmissible cancer shifts from emergence to endemism in Tasmanian devils. *Science*, 370, eabb9772.

Pearse, A.M. & Swift, K. (2006). Allograft theory: Transmission of devil facial-tumour disease. *Nature*, 439, 549.

Pettit, L.I. (1990). The conditional predictive ordinate for the normal distribution. *J. Roy. Stat. Soc.: Ser. B (Methodol.)*, 52, 175–184.

Plowright, R.K., Becker, D.J., McCallum, H. & Manlove, K.R. (2019). Sampling to elucidate the dynamics of infections in reservoir hosts. *Philos. Trans. R. Soc. B Biol. Sci.*, 374, 20180336.

Pye, R., Hamede, R., Siddle, H.V., Caldwell, A., Knowles, G.W., Swift, K. *et al.* (2016a). Demonstration of immune responses against devil facial tumour disease in wild Tasmanian devils. *Biol. Let.*, 12, 20160553.

Pye, R.J., Pemberton, D., Tovar, C., Tubio, J.M.C., Dun, K.A., Fox, S. *et al.* (2016b). A second transmissible cancer in Tasmanian devils. *Proc. Natl Acad. Sci.*, 113, 374–379.

R Core Team (2019). *R: A Language and Environment for Statistical Computing*. R Foundation for Statistical Computing, Vienna, Austria.

Rue, H., Martino, S. & Chopin, N. (2009). Approximate Bayesian inference for latent Gaussian models by using integrated nested Laplace approximations. *J. R. Stat. Soc. Series B Stat. Methodol.*, 71, 319–392.

Ruiz-Aravena, M., Jones Menna, E., Carver, S., Estay, S., Espejo, C., Storfer, A. *et al.* (2018). Sex bias in ability to cope with cancer: Tasmanian devils and facial tumour disease. *Proc. R. Soc. B Biol. Sci.*, 285, 20182239.

Russell, C.A., Smith, D.L., Childs, J.E. & Real, L.A. (2005). Predictive spatial dynamics and strategic planning for raccoon rabies emergence in Ohio. *PLoS Biol.*, 3(3), e88.

Skerratt, L.F., Berger, L., Speare, R., Cashins, S., McDonald, K.R., Phillott, A.D. *et al.* (2007). Spread of chytridiomycosis has caused the rapid global decline and extinction of frogs. *EcoHealth*, 4, 125.

Smith, D.L., Lucey, B., Waller, L.A., Childs, J.E. & Real, L.A. (2002). Predicting the spatial dynamics of rabies epidemics on heterogeneous landscapes. *Proc. Natl Acad. Sci.*, 99, 3668–3672.

Smith, D.L., Waller, L.A., Russell, C.A., Childs, J.E. & Real, L.A. (2005). Assessing the role of long-distance translocation and spatial heterogeneity in the raccoon rabies epidemic in Connecticut. *Prev. Vet. Med.*, 71, 225–240.

Storfer, A., Epstein, B., Jones, M., Micheletti, S., Spear, S.F., Lachish, S. *et al.* (2017). Landscape genetics of the Tasmanian devil: implications for spread of an infectious cancer. *Conserv. Genet.*, 18, 1287–1297.

Swinton, J., Harwood, J., Grenfell, B.T. & Gilligan, C.A. (1998). Persistence thresholds for phocine distemper virus infection in harbour seal *Phoca vitulina metapopulations*. *J. Anim. Ecol.*, 67, 54–68.

Theobald, E.J., Ettinger, A.K., Burgess, H.K., DeBey, L.B., Schmidt, N.R., Froehlich, H.E. *et al.* (2015). Global change and local solutions: Tapping the unrealized potential of citizen science for biodiversity research. *Biol. Cons.*, 181, 236–244.

Watson, J., Joy, R., Tollit, D., Thornton, S. & Auger-Methe, M. (2019). A general framework for estimating the spatio-temporal distribution of a species using multiple data types. *arXiv preprint arXiv:1911.00151*.

Wells, K., Hamede, R.K., Jones, M.E., Hohenlohe, P.A., Storfer, A. & McCallum, H.I. (2019). Individual and temporal variation in pathogen load predicts long-term impacts of an emerging infectious disease. *Ecology*, 100, e02613.

White, L.A., Forester, J.D. & Craft, M.E. (2018). Dynamic, spatial models of parasite transmission in wildlife: their structure, applications and remaining challenges. *J. Anim. Ecol.*, 87, 559–580.

Woodroffe, R., Donnelly, C.A., Cox, D.R., Bourne, F.J., Cheeseman, C.L., Delahay, R.J. *et al.* (2006). Effects of culling on badger *Meles meles* spatial organization: implications for the control of bovine tuberculosis. *J. Appl. Ecol.*, 43, 1–10.

SUPPORTING INFORMATION

Additional supporting information may be found online in the Supporting Information section at the end of the article.